

FLAME: A Federated Learning Approach for Multi-Modal RF Fingerprinting

Kiarash Kianfar and Rajeev Sahay

Abstract—Authorization systems are increasingly relying on processing radio frequency (RF) waveforms at receivers to fingerprint (i.e., determine the identity) of the corresponding transmitter. Federated learning (FL) has emerged as a popular paradigm to perform RF fingerprinting in networks with multiple access points (APs), as they allow effective deep learning-based device identification without requiring the centralization of locally collected RF signals stored at multiple APs. Yet, FL algorithms that operate merely on in-phase and quadrature (IQ) time samples incur high convergence rates, resulting in excessive training rounds and inefficient training times. In this work, we propose FLAME: an FL approach for multimodal RF fingerprinting. Our framework consists of simultaneously representing received RF waveforms in multiple complimentary modalities beyond IQ samples in an effort to reduce training times. We theoretically demonstrate the feasibility and efficiency of our methodology and derive a convergence bound that incurs lower loss and thus higher accuracies in the same training round in comparison to single-modal FL-based RF fingerprinting. Extensive empirical evaluations validate our theoretical results and demonstrate the superiority of FLAME with improvements of up to 30% in comparison to multiple considered baselines.

Index Terms—Federated learning, multi-modal federated learning, physical-layer communications, rf fingerprinting.

I. INTRODUCTION

ALL pieces of transmitting hardware inherently contain slight physical differences due to imperfections in their manufacturing processes. Due to these hardware imperfections, radio transmitters have slight variations in their transmitted radio frequency (RF) waveforms, reflected in the channel state information (CSI) of the received signal [1]. RF fingerprinting is a technique that utilizes these unchanging variations in transmitted signals to identify the transmitting device. Such RF fingerprinting techniques are vital in both military and civilian applications, where accurate device identification is required to prevent receivers from servicing unauthorized or adversarial transmitters [2].

Current state-of-the-art methods for RF fingerprinting are largely comprised of deep learning approaches [3]–[7], which significantly outperform statistical signal processing methods such as maximum likelihood classifiers [8]–[10]. However, deep learning approaches are difficult to scale in next-generation communications, where radio waveforms are typically stored at multiple access points (APs) within a wireless network and require the aggregation of gigabytes to terabytes

of data to a centralized location before model training can occur. Not only would such data aggregation be computationally costly, but it also increases the potential of data leakage during the aggregation process.

Federated learning (FL), a distributed and privacy-preserving deep learning paradigm, has recently emerged as a potential solution for RF fingerprinting to mitigate the challenges of centralized deep learning approaches [11]–[13]. The FL RF fingerprinting approach trains local models at each AP on locally stored RF data at each AP. Each AP, after performing local training, then transmits only the updated model parameters (which are often much smaller than the size of the fingerprinting data) to a centralized location (e.g., a coordinating server) for aggregation. The central server then aggregates its received model parameters into a global model and transmits the updated parameters of the global model to each AP to resume the training process. In this fashion, the locally collected fingerprinting data at each AP never leaves its stored location, reducing communication overhead and improving data security.

Despite its benefits, federated learning poses two key challenges in large-scale RF fingerprinting networks. First, RF fingerprinting data across APs are often heterogeneous and, thus, each AP only contains fingerprinting data corresponding to a subset of transmitters attempting to be learned by the global model. As a result, the global model struggles to generalize to all transmitters, impeding overall performance. Second, the central server in FL requires frequent aggregation from each AP, directly incurring high communication overhead. Together, these challenges require performing (i) a low number of model parameter updates during each training round to prevent the weights of each local model from diverging too significantly from the global model [14] and (ii) a large number of FL training iterations [15] in order to achieve high RF fingerprinting performance.

In this work, we develop an FL approach for multimodal RF fingerprinting (FLAME). FLAME consists of using complimentary signal information at each AP, in the form of multiple signal modalities, to perform local training prior to global aggregation. We show that, under our proposed framework, the variance of the global loss is proportionally reduced by a factor consistent with the number of modalities used at each AP. As a result, a larger number of local parameter updates can occur at each AP in FLAME, since the variance of the aggregated loss is reduced in comparison to using a single modality. In addition, the FLAME training process requires fewer communication rounds between APs and the central server since the variance of the loss at each AP is reduced, thus

K. Kianfar and R. Sahay are with the Department of Electrical and Computer Engineering, UC San Diego, San Diego, CA, 92093 USA. E-mail: {kkianfar,r2sahay}@ucsd.edu.

This work was supported in part by the UC San Diego Academic Senate under grant RG114404.

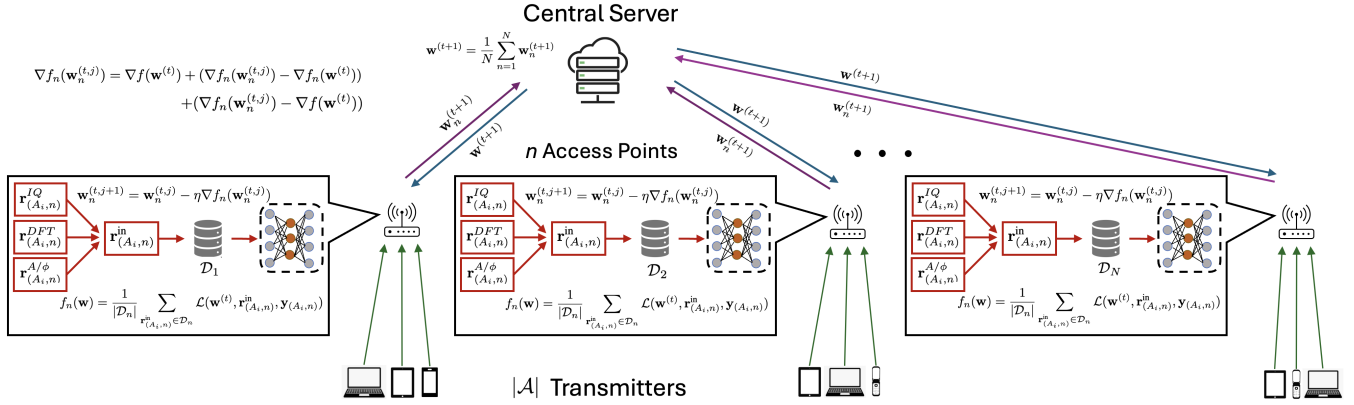


Fig. 1: The FLAME system diagram consisting of n access points (APs) servicing $|\mathcal{A}|$ transmitters.

increasing the tolerance with which the weights of the local models can diverge prior to global aggregation. We theoretically and empirically show the benefits of FLAME in terms of efficiency and fingerprinting performance in comparison to previously proposed FL approaches for RF fingerprinting.

Summary of Contributions: Our contributions, in comparison to related work (discussed in Sec. II), can be summarized as follows:

- 1) **Development of FLAME** (Sec. III-A – Sec. III-C): We develop an efficient FL approach for multimodal RF fingerprinting (FLAME) that mitigates the challenges induced in traditional FL-based device identification. *To the best of our knowledge, this is the first framework to develop a multimodal framework for FL-based RF fingerprinting.*
- 2) **Theoretical Feasibility of FLAME** (Sec. III-D): We theoretically show the feasibility of FLAME. Specifically, we show that our proposed framework converges faster and attains higher fingerprinting performance in comparison to previously proposed FL approaches for RF fingerprinting.
- 3) **Empirical Evaluation** (Sec. IV-A – IV-D): We perform an empirical analysis to confirm our theoretical results. We show that FLAME achieves higher performance rates in fewer training iterations than the considered baselines on a real-world RF fingerprinting dataset.

II. RELATED WORKS

RF fingerprinting primarily relies on performing device authentication based on the transient response of RF signals [16]. Early classification methods consisted of correlation detection [17], signal strength measurements from multiple access points [18], and maximum likelihood approaches [8]–[10]. However, such methods struggle to yield high accuracy for effective device classification. Recent data-driven machine learning approaches, on the other hand, have been successful in achieving high RF fingerprinting performance directly on the transient response of received signals [3]–[7], [19], [20]. Yet, these methods primarily rely on the traditional, centralized training approach, which has potential limitations. Specifically, the aggregation of RF data from multiple wireless access

points is not feasible for large local datasets and increases chances of data leakage, raising privacy and security concerns.

Federated learning (FL) has emerged as a promising distributed RF fingerprinting approach, allowing for model training at local access points directly thus eliminating the need for data centralization. Multiple frameworks for FL have been explored for RF fingerprinting [11]–[13] as well as long-range (LoRa) communications [21]. These studies have shown the improvements of FL in terms of data privacy. However, FL has shown lower performance than centralized training due to the heterogeneity of data distributions at various access points as well as the reliance on single-modal (i.e., IQ-based) processing as opposed to multi-modal-based FL as we propose.

Meanwhile, separate studies have worked with multi-modal RF data, showing the performance improvements obtained by utilizing multiple modalities of the same data for centralized deep learning, primarily for automatic modulation classification (AMC) [22]–[24], but also for RF fingerprinting [25]. Multi-modal-based FL approaches have also emerged in various applications outside of wireless communications, improving FL performance, compared to single-modal training, in a variety of settings [26]–[28]. However, multi-modal FL, encompassing its unique challenges such as data heterogeneity across access points, has not been explored for RF fingerprinting. Thus, in this work, we propose the first multi-modal-based FL framework for RF fingerprinting and demonstrate its efficacy both theoretically and empirically.

III. METHODOLOGY

Here, we state our signal model (Sec. III-A) and describe our multimodal (Sec. III-B) and federated learning (FL) framework (Sec. III-C). We then demonstrate the feasibility of our methodology through a convergence analysis (Sec. III-D). An overview of our FLAME methodology is shown in Fig. 1.

A. Signal Modeling

We consider an FL framework consisting of $\mathcal{A} = \{A_1, A_2, \dots, A_{|\mathcal{A}|}\}$ transmitters and $n = 1, 2, \dots, N$ Access Points (APs), where each AP contains a local dataset denoted by \mathcal{D}_n consisting of $|\mathcal{D}_n|$ samples. At each AP, \mathcal{D}_n is comprised of a set of signals, received from a subset of

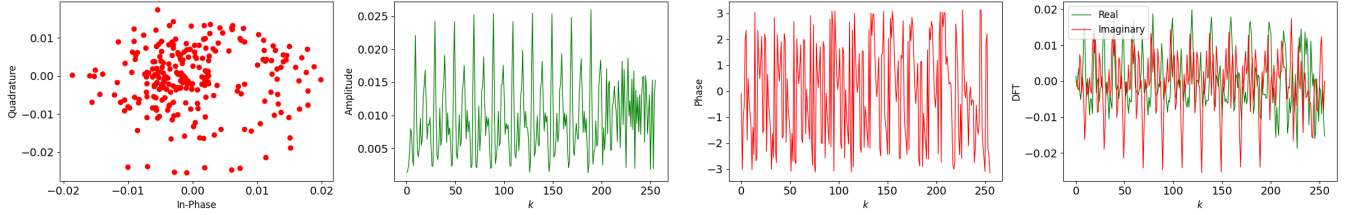


Fig. 2: A visualization of each considered modality, which shows Modality 1 (first), Modality 2 (second), and Modality 3 (third and fourth).

transmitters $\mathcal{A}_n = \{A_1, A_2, \dots, A_{|\mathcal{A}_n|}\}$, where $\mathcal{A}_n \subset \mathcal{A}$ and, thus, $|\mathcal{A}_n| < |\mathcal{A}|$. We further assume that each transmitter is only serviced by a single and unique AP and, therefore, $\mathcal{D}_1 \cap \mathcal{D}_2 \cap \dots \cap \mathcal{D}_N = \emptyset$. Here, we consider two distinct scenarios: (i) $\mathcal{A}_1 \cap \mathcal{A}_2 \cap \dots \cap \mathcal{A}_N = \emptyset$ and (ii) $\mathcal{A}_1 \cap \mathcal{A}_2 \cap \dots \cap \mathcal{A}_N \neq \emptyset$. Practically, (i) corresponds to non-independent and identically distributed (non i.i.d.) transmitters, where each AP only receives transmissions from a specific subset of transmitters and is thus only exposed to a subset of transmitter fingerprints, and (ii) corresponds to an i.i.d. setting, where a transmitter may transmit to different APs and thus multiple APs contain fingerprints from multiple transmitters.

Formally, the received signal from the i^{th} transmitter, A_i , at AP n is modeled by

$$\mathbf{r}_{(A_i, n)} = h_{A_i}(\mathbf{s}, t) + \mathbf{n}, \quad (1)$$

where $\mathbf{r}_{(A_i, n)} = [r_{(A_i, n)}[0], \dots, r_{(A_i, n)}[\ell - 1]]^T \in \mathbb{C}^\ell$, ℓ is the length of the received signal's observation window, $\mathbf{n} \in \mathbb{C}^\ell$ represents complex additive white Gaussian noise (AWGN), \mathbf{s} is the set of transmitted symbols and h_{A_i} represents the time-variant RF fingerprint (of A_i), which captures the transmitter hardware fingerprints and wireless channel effects. We assume that the channel distribution between each transmitter and its receiving AP is i.i.d. The FL objective is to learn a global RF fingerprinting classifier to predict $A_i \in \mathcal{A}$, given $\mathbf{r}_{(A_i, n)}$, by training all local models at each AP.

B. Multi-Modal Domain Representations

We represent each received signal, $\mathbf{r}_{(A_i, n)}$, in three different modalities in order to model each signal using discriminative features for accurate RF fingerprinting. Specifically, we consider the (i) in-phase and quadrature (IQ) time-domain representation of the received signal at complex baseband, (ii) frequency-domain representation obtained via the Discrete Fourier Transform (DFT) of the received complex baseband signal, and (iii) amplitude and phase of the received complex baseband signal. Each representation has been independently used to perform classification in various wireless settings, including, but not limited to RF fingerprinting [24], [29], but no work has jointly used all three considered modalities for RF fingerprinting. We detail our methodology used to arrive at each of the specific modalities below.

Modality 1 We first model each received signal, $\mathbf{r}_{(A_i, n)} \in \mathbb{C}^\ell$, in its baseband form. Following prior work [12], [30], we map each baseband IQ signal to a two-dimensional real matrix, $\mathbf{r}_{(A_i, n)} \in \mathbb{C}^\ell \rightarrow \mathbf{r}_{(A_i, n)}^{\text{IQ}} \in \mathbb{R}^{\ell \times 2}$ where the first and second column of $\mathbf{r}_{(A_i, n)}^{\text{IQ}}$ represent the real and imaginary

components, respectively, of $\mathbf{r}_{(A_i, n)}$ so that they can be used with real-valued neural networks.

Modality 2 Next, we model $\mathbf{r}_{(A_i, n)} = [r_t[0], \dots, r_t[\ell - 1]]^T$ using the frequency components obtained from its discrete Fourier transform (DFT). Specifically, the p^{th} frequency component of the DFT of $\mathbf{r}_{(A_i, n)}$ is given by

$$\mathbf{R}_{(A_i, n)}[p] = \sum_{k=0}^{\ell-1} \mathbf{r}_{(A_i, n)}[k] e^{-\frac{j2\pi}{\ell} pk}, \quad p = 0, \dots, \ell - 1, \quad (2)$$

where $\mathbf{R}_{(A_i, n)} = [\mathbf{R}_{(A_i, n)}[0], \dots, \mathbf{R}_{(A_i, n)}[\ell - 1]]^T \in \mathbb{C}^\ell$ contains all frequency components of $\mathbf{r}_{(A_i, n)}$. Similar to Modality 1, we map $\mathbf{R}_{(A_i, n)}$ to a two-dimensional real matrix, $\mathbf{R}_{(A_i, n)} \in \mathbb{C}^\ell \rightarrow \mathbf{r}_{(A_i, n)}^{\text{DFT}} \in \mathbb{R}^{\ell \times 2}$ where the first and second column of $\mathbf{r}_{(A_i, n)}^{\text{DFT}}$ represent the real and imaginary components, respectively, of $\mathbf{R}_{(A_i, n)}$.

Modality 3 Finally, we model $\mathbf{r}_{(A_i, n)}$ using its amplitude and phase for each time sample. Specifically, we determine

$$r_{(A_i, n)}^A[k] = \sqrt{(\Re(r_{(A_i, n)}[k]))^2 + (\Im(r_{(A_i, n)}[k]))^2} \quad (3)$$

and

$$r_{(A_i, n)}^\phi[k] = \tan^{-1} \left(\frac{\Im(r_{(A_i, n)}[k])}{\Re(r_{(A_i, n)}[k])} \right) \quad (4)$$

for $k = 0, \dots, \ell - 1$, where $\Re(\cdot)$ and $\Im(\cdot)$ represent the real and imaginary component of (\cdot) , respectively. For each signal, $\mathbf{r}_{(A_i, n)}$, we store the result of (3) and (4) in a real-valued two-dimensional matrix denoted by $\mathbf{r}_{(A_i, n)}^{A/\phi} \in \mathbb{R}^{\ell \times 2}$, where the first and second column of $\mathbf{r}_{(A_i, n)}^{A/\phi}$ represent the amplitude and phase, respectively, of $\mathbf{r}_{(A_i, n)}$.

Fig. 2 visualizes examples of $\mathbf{r}_{(A_i, n)}^{\text{IQ}}$, $\mathbf{r}_{(A_i, n)}^{\text{DFT}}$, and $\mathbf{r}_{(A_i, n)}^{A/\phi}$ for signals received with various RF fingerprints. For each local dataset at AP n , we compute an M channel input for each signal, denoted by $\mathbf{r}_{(A_i, n)}^{\text{in}} \in \mathbb{R}^{\ell \times 2 \times M}$, where M denotes the number of modalities concatenated together (e.g., jointly using Modality 1, 2, and 3 would result in $M = 3$ since three modalities are used).

C. Classifier Modeling

We denote a deep learning classifier as $z_{\mathbf{w}} : \mathbf{r}_{(A_i, n)}^{\text{in}} \rightarrow \hat{\mathbf{y}}_{(A_i, n)}$, where the classifier is parametrized by \mathbf{w} and trained to fingerprint the input, $\mathbf{r}_{(A_i, n)}^{\text{in}} \in \mathbb{R}^{\ell \times 2 \times M}$, to $\hat{\mathbf{y}}_{(A_i, n)} \in \mathbb{R}^{|\mathcal{A}|}$, which denotes the predicted transmitter. Each AP shares the same deep learning architecture. The objective of the FL network is to find \mathbf{w} that minimizes the loss between $\hat{\mathbf{y}}_{(A_i, n)}$ and

the true transmitter $\mathbf{y}_{(A_i,n)}$. Formally, this can be expressed as

$$\min_{\mathbf{w}} f(\mathbf{w}), \quad \text{where } f(\mathbf{w}) := \frac{1}{N} \sum_{n=1}^N f_n(\mathbf{w}), \quad (5)$$

$$f_n(\mathbf{w}) = \frac{1}{|\mathcal{D}_n|} \sum_{\mathbf{r}_{(A_i,n)}^{\text{in}} \in \mathcal{D}_n} \mathcal{L}(\mathbf{w}^{(t)}, \mathbf{r}_{(A_i,n)}^{\text{in}}, \mathbf{y}_{(A_i,n)}) \quad (6)$$

and $\mathcal{L}(\mathbf{w}^{(t)}, \mathbf{r}_{(A_i,n)}^{\text{in}}, \mathbf{y}_{(A_i,n)})$ is the local loss function at AP n over \mathcal{D}_n .

Since the fingerprinting data is distributed among N access points, (5) is achieved through multiple rounds of local learning, parameter aggregation, and global model synchronization. Specifically, at the beginning of each training round, t , the global model transmits its parameters, $\mathbf{w}^{(t)}$, to each AP. AP n then initializes $\mathbf{w}_n^{(t,0)} = \mathbf{w}^{(t)}$ and trains its local model by minimizing its local loss using \mathcal{D}_n , in which each input signal is constructed by concatenating M modalities, using J stochastic gradient descent (SGD) steps according to

$$\mathbf{w}_n^{(t,j+1)} = \mathbf{w}_n^{(t,j)} - \eta \nabla f_n(\mathbf{w}_n^{(t,j)}), \quad (7)$$

where $j = 0, \dots, J-1$, ∇ represents the gradient with respect to $\mathbf{w}_n^{(t,j)}$, and η is the learning rate. Since the local model at AP n is trained on instances of $\mathbf{r}_{(A_i,n)}^{\text{in}}$, which contain M modalities, $\mathbf{w}_n^{(t+1)}$ accounts for the updated loss from M modalities simultaneously.

At the termination of the training round, each local device sets $\mathbf{w}_n^{(t+1)} = \mathbf{w}_n^{(t,J)}$ and returns $\mathbf{w}_n^{(t+1)}$, which are the model parameters of AP n after the completion of training round t on \mathcal{D}_n , to the global server. The global server then performs parameter aggregation by calculating the parameters for the next training iteration according to

$$\mathbf{w}^{(t+1)} = \frac{1}{N} \sum_{n=1}^N \mathbf{w}_n^{(t+1)}. \quad (8)$$

After aggregation, the global server transmits the updated model parameters, $\mathbf{w}^{(t+1)}$, for the next round of training to each AP. This process continues for T training iterations. Our complete FLAME methodology for a single training iteration of RF fingerprinting is detailed in Algorithm 1.

D. Convergence Analysis

Here, we will analyze the convergence of Algorithm 1 by deriving a lower bound that demonstrates the convergence efficiency of our proposed methodology. We will employ the following common assumptions in our analysis:

Assumption 1 (Smoothness). The local objective function $f_n(\mathbf{w})$ is L -Lipschitz smooth such that $f_n(\mathbf{w}') \leq f_n(\mathbf{w}) + \langle \nabla f_n(\mathbf{w}), \mathbf{w}' - \mathbf{w} \rangle + L/2 \|\mathbf{w}' - \mathbf{w}\|^2$ is satisfied for any two parameters \mathbf{w} and \mathbf{w}' .

Assumption 2 (Bounded gradient variance). For stochastic gradients at each AP (which arise from sampling random mini-batches during local training), $\mathbb{E}[\|\nabla f_n(\mathbf{w}_n^{(t,j)}) - \nabla f_n(\mathbf{w}_n)\|^2] \leq \sigma^2/M$ for $M > 1$, where σ^2 is the variance of the stochastic gradients when a single modality is used.

Algorithm 1 FLAME methodology at training iteration $t > 0$

```

1: input:  $\mathbf{w}^{(t)}$ : global parameters at training iteration  $t$ 
    $B$ : batch size
    $J$ : SGD iterations
    $\eta$ : learning rate at each AP
2: for  $n = 1, \dots, N$  (in parallel) do
3:   for each  $\mathbf{r}_{(A_i,n)} \in \mathcal{D}_n$  do
4:     compute  $\mathbf{r}_{(A_i,n)}^{\text{IQ}}, \mathbf{r}_{(A_i,n)}^{\text{DFT}}, \mathbf{r}_{(A_i,n)}^{\text{A}/\phi} \in \mathbb{R}^{\ell \times 2}$ 
5:     construct  $\mathbf{r}_{(A_i,n)}^{\text{in}} \in \mathbb{R}^{\ell \times 2 \times M}$  where  $M = 3$ 
6:      $\mathcal{D}_n = \mathcal{D}_n \setminus \{\mathbf{r}_{(A_i,n)}\}$ 
7:      $\mathcal{D}_n = \mathcal{D}_n \cup \{\mathbf{r}_{(A_i,n)}^{\text{in}}\}$ 
8:   end for
9:    $\mathbf{w}_n^{(t,0)} \leftarrow \mathbf{w}^{(t)}$ 
10:  for  $j = 0, 1, \dots, J-1$  do
11:    form mini-batch of  $B$  random samples  $\mathcal{B}_n^{(j)} \subseteq \mathcal{D}_n$ 
12:     $f_n(\mathbf{w}) = \frac{1}{|\mathcal{B}_n^{(j)}|} \sum_{\mathbf{r}_{(A_i,n)}^{\text{in}} \in \mathcal{B}_n^{(j)}} \mathcal{L}(\mathbf{w}^{(t)}, \mathbf{r}_{(A_i,n)}^{\text{in}}, \mathbf{y}_{(A_i,n)})$ 
13:     $\mathbf{w}_n^{(t,j+1)} \leftarrow \mathbf{w}_n^{(t,j)} - \eta \nabla f_n(\mathbf{w}_n^{(t,j)})$ 
14:  end for
15:   $\mathbf{w}_n^{(t+1)} \leftarrow \mathbf{w}_n^{(t,J)}$ 
16: end for
17:  $\mathbf{w}^{(t+1)} = \frac{1}{N} \sum_{n=1}^N \mathbf{w}_n^{(t+1)}$ 
18: return  $\mathbf{w}^{(t+1)}$ 

```

Assumption 3 (Bounded AP drift). The differences between local gradients (drift) across all APs satisfies $\mathbb{E}[\|\nabla f_n(\mathbf{w}^{(t)}) - \nabla f(\mathbf{w}^{(t)})\|^2] \leq \zeta^2/M$ for $M > 1$, where ζ^2 is the variance of the gradients across APs due to the differences in their local data distributions when a single modality is used.

Assumption 4 (Convexity). The global objective $f(\mathbf{w})$ is μ -strongly convex such that $f(\mathbf{w}') \geq f(\mathbf{w}) + \langle \nabla f(\mathbf{w}), \mathbf{w}' - \mathbf{w} \rangle + \mu/2 \|\mathbf{w}' - \mathbf{w}\|^2$ is satisfied for any two parameters \mathbf{w} and \mathbf{w}' .

Next, we present the following lemma, which represents the true local loss and accounts for the loss at each AP as well as the deviation of the local loss from the true global loss and stochastic noise.

Lemma 1. *The local loss gradient, defined by $\nabla f_n(\mathbf{w}_n^{(t,j)})$ can be decomposed into the following expression:*

$$\begin{aligned} \nabla f_n(\mathbf{w}_n^{(t,j)}) &= \nabla f(\mathbf{w}^{(t)}) + (\nabla f_n(\mathbf{w}_n^{(t,j)}) - \nabla f_n(\mathbf{w}^{(t)})) \\ &\quad + (\nabla f_n(\mathbf{w}_n^{(t,j)}) - \nabla f(\mathbf{w}^{(t)})), \end{aligned} \quad (9)$$

where $\nabla f_n(\mathbf{w}_n^{(t,j)}) - \nabla f_n(\mathbf{w}^{(t)})$ represents the stochastic gradient noise, which arises from local training on random mini-batches and $\nabla f_n(\mathbf{w}_n^{(t,j)}) - \nabla f(\mathbf{w}^{(t)})$ represents the heterogeneity present at each AP (i.e., the deviation of the local gradient from the global gradient) due to the difference in data distributions at each AP.

Proof. See Appendix A. \square

Given Assumptions 1 – 4 as well as Lemma 1, and without loss of generality, we present the following theorem, which provides a lower bound on the convergence of our methodology as a function of the number of modalities M .

Theorem 1. With $f_n(\mathbf{w})$ satisfying Assumptions 1 – 4, and setting $f^* = \min_{\mathbf{w}} f(\mathbf{w})$ (i.e., f^* is the value of $f(\mathbf{w})$ at the optimal solution \mathbf{w}^* , which minimizes (5)), the convergence rate of Algorithm 1 is bounded by

$$\mathbb{E}[f(\mathbf{w}^{(t+1)}) - f^*] \leq \mathbb{E}[f(\mathbf{w}^{(t)}) - f^*] \left(1 - \frac{\eta J \mu}{M}\right) + \frac{\eta^2 L J^2 (\sigma^2 + \zeta^2)}{2NM}. \quad (10)$$

Proof. See Appendix B. \square

Theorem 1 provides a bound on how the global loss is affected for an RF fingerprinting network consisting of N APs that are trained using M modalities. In particular, we observe that (i) the variance terms are scaled down by M due to the input containing multiple representations, which capture complimentary signal features and aid in faster convergence across APs and (ii) the bound is a function of $(\sigma^2 + \zeta^2)/M$, which directly shows the improvement in convergence when $M > 1$ as proposed in FLAME, and (iii) the term $1 - (\eta J \mu)/M$, which determines the decrease of the loss in each iteration, is a function of $1/M$ and is guaranteed to decrease when multiple modalities are used (i.e., when $M > 1$) in comparison to when a single modality is used (i.e., when $M = 1$). Finally, note that Theorem 1 does not make any prior assumptions about the similarity (or dissimilarity) of data distributions at each AP. Thus, from Theorem 1, we see that FLAME is guaranteed to improve the global convergence rate across the network of APs regardless of the extent of non-i.i.d. behaviors among APs.

IV. PERFORMANCE EVALUATION

In this section, we describe our empirical setup including our employed dataset as well as our FL architecture (Sec. IV-A). Next, we show the efficacy of our framework on both i.i.d. (Sec. IV-B) and non i.i.d. (Sec. IV-C) signal environments. Finally, we further improve the performance of FLAME using personalized FL, where we fine tune the fingerprinting model at each AP (Sec. IV-D).

A. Experimental Setup

We employ the open source RF fingerprinting dataset presented in [31] for our empirical analysis. The wireless setup used $|\mathcal{A}| = 163$ WiFi modules as transmitters and a software defined radio (USRP N210) as a receiver. The transmitted data had a center frequency of 2462 MHz and a bandwidth of 20 MHz. In addition, the received waveforms used for training consisted of $\ell = 256$ IQ samples, capturing the received signal’s preamble, which can be used in place of the entire received payload to perform effective device RF fingerprinting without incurring unnecessary training overhead [32], [33].

Our FL architecture consisted of using ResNet classifiers [34], whose architecture is shown in Table I. In addition, we used the following hyperparameter values in our empirical evaluation: $N = 4$, $B = 512$, $J = 100$, $\eta = 0.001$, and $T = 1000$.

TABLE I: The layers, along with their corresponding output shapes, of our CNN architecture.

Layer	Activation Function	Output Shape
Input	-	$256 \times 2 \times 1$
Residual Block 1	-	$256 \times 2 \times 16$
Max Pooling 2×1	-	$128 \times 2 \times 16$
Residual Block 2	-	$128 \times 2 \times 32$
Max Pooling 2×1	-	$64 \times 2 \times 32$
Conv2D	Softmax	$64 \times 2 \times 16$
Fully Connected	ReLU	80
Fully Connected	Softmax	163

TABLE II: The layers in our residual block. The Add Conv2D 1 represents the residual skip connection.

Layer	Output Shape
Conv2D 1	$256 \times 2 \times 16$
Conv2D 2	$256 \times 2 \times 16$
BatchNorm 1	$256 \times 2 \times 16$
ReLU	$256 \times 2 \times 16$
Conv2D 3	$256 \times 2 \times 16$
BatchNorm 2	$256 \times 2 \times 16$
Add Conv2D 1 (Skip)	$256 \times 2 \times 16$
ReLU	$256 \times 2 \times 16$

B. i.i.d. Results

Here, we consider an i.i.d. setting using $M = 3$, which consists of Modality 1, Modality 2, and Modality 3. In this setting, we use $|\mathcal{D}_n| = 76.3K \forall n$ training samples consisting of waveforms received from each transmitter. Thus, each AP performs local training on $|\mathcal{A}_n| = 163$ transmitters. The central server contains 83.8K testing signals (not present in $\mathcal{D}_n \forall n$), corresponding to all $|\mathcal{A}_n| = 163$ transmitters, which are used to evaluate the global model at the conclusion of training round t .

We compare the performance of our proposed methodology to single modal-based FL for RF fingerprinting [11]–[13], where only IQ samples are used for training at each AP. For completeness, we extend the methodologies of these works and consider their proposed approaches when single-modal signals other than IQ signals are used for training (i.e., received signals processed via (2) or (3) and (4)), presented as Modality 2 and Modality 3 in our work).

We show the evolution of FLAME, in comparison to the considered baselines, in Fig. 3 under the i.i.d. FL scenario. From 3, we see that our proposed framework outperforms each considered baseline at the time of convergence. In particular, FLAME significantly outperforms previously proposed FL approaches that merely rely on IQ features for RF fingerprinting. In addition, we see from Fig. 3 that single-modal data based on Modality 2 achieves convergence in fewer training iterations compared to FLAME (although to a lower overall classification performance). This suggests that the fingerprinting characteristics captured in each received signal’s CSI contains more discernible features in its frequency components in comparison to IQ features in FL based RF device identification. This insight is further corroborated in Sec. IV-C below.

In Fig. 4, we show the training evolution of FLAME in comparison to different multimodal combinations, using

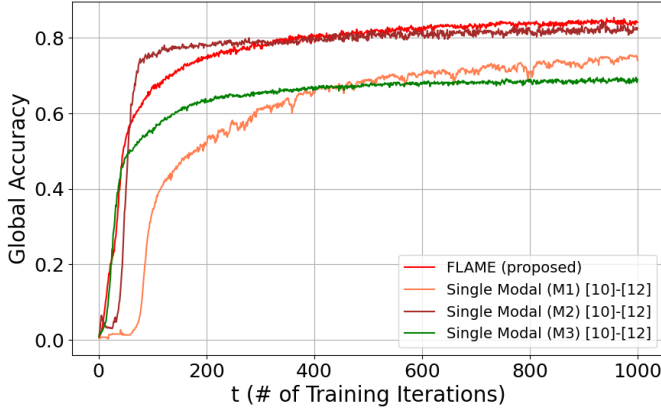


Fig. 3: The performance of our proposed method in comparison to the considered baseline approaches in the i.i.d. setting. Here, we see that FLAME outperforms all considered baselines in which single modal training is used.

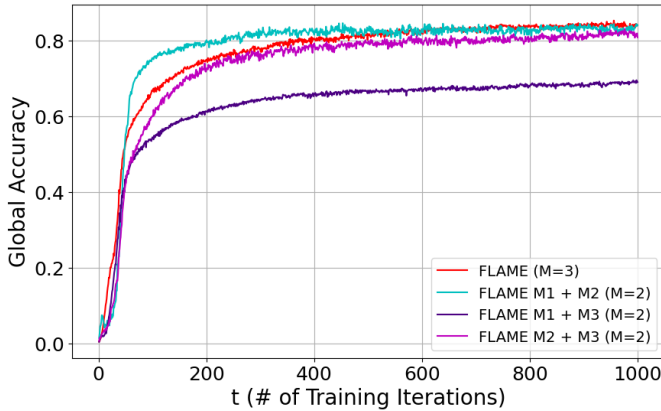


Fig. 4: A comparison of different variations of FLAME in the i.i.d. setting. Although performance was similar, we can see that FLAME with $M=3$ manages to outperform the other variations by convergence.

Modality 1, Modality 2, and Modality 3, in the i.i.d. setting using $M = 2$ in order to further empirically validate Theorem 1. In this case, FLAME continues to outperform each considered baseline with combinations containing Modality 2 being closest in final global convergence to FLAME. This behavior is consistent with that seen in Fig. 3, where data containing frequency-based features are more important for RF fingerprinting in comparison to features in other considered modalities. Furthermore, we see in Fig. 3 that the performance of other multimodal approaches, where $M = 2$ is closer in global performance to FLAME. This behavior is consistent with Theorem 1 as well as Assumption 2 and Assumption 3 in which the variance of the loss’s gradient scales with the number of modalities M , thus improving FLAME as M increases.

C. Non i.i.d Results

Here, we consider a non i.i.d. setting using $M = 3$, which consists of Modality 1, Modality 2, and Modality 3. In this setting, similar to the i.i.d setting, we use $|\mathcal{D}_n| = 76.3K \forall n$



Fig. 5: The performance of our proposed method in comparison to the considered baseline approaches in the non-i.i.d. setting. Similar to Fig. 3, we see that FLAME outperforms all considered baselines in which single modal training is used.

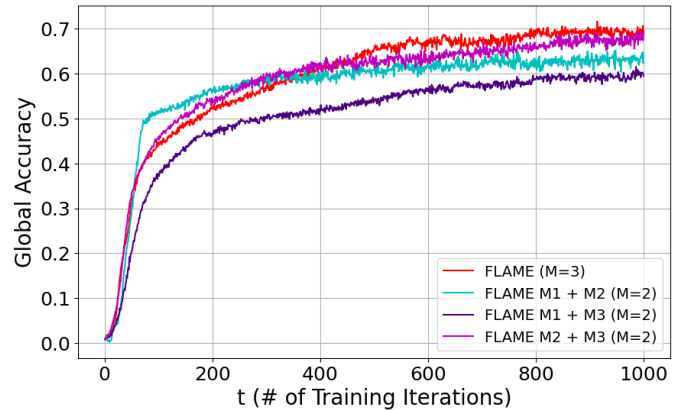


Fig. 6: A comparison of different variations of FLAME in the non-i.i.d. setting. Here, the performance increase from the $M=2$ variations to $M=3$ is slightly more pronounced than in Fig. 4.

training samples at each AP. However, in the non i.i.d. setting, we use $|\mathcal{A}_n| = 41$ at each AP. In this case, almost all APs only contain waveforms from unique transmitters, and select transmitters (no more than one overlapping transmitter per AP pair) have communicated with two APs, thus resulting in significant heterogeneity in the distributions of \mathcal{D}_n across APs. The central server contains 83.8K testing signals (not present in $\mathcal{D}_n \forall n$), corresponding to all $|\mathcal{A}_n| = 163$ transmitters, which are used to evaluate the global model at the conclusion of training round t similar to the i.i.d scenario.

Fig. 5 shows the performance of FLAME in comparison to the considered baselines for the non i.i.d. setting. Similar to the i.i.d. scenario, FLAME converged to the highest global accuracy in comparison to each considered baseline. In particular, traditional FL approaches for RF fingerprinting using only IQ features for training attain the lowest performance, failing to achieve a global accuracy over 45% in any training iteration whereas FLAME attains a final global accuracy that is nearly 35% higher. Here, in the non i.i.d. scenario, the complimentary signal information presented in multiple modalities, as proposed in FLAME, is especially important to

TABLE III: The classification performance of each AP in the i.i.d. setting. We see that before personalized FL, each AP has the same classification performance (since all AP's have the same global testing set in the i.i.d. case), whereas after personalized FL, the local model at each AP improves on the global testing set (nearly to the same extent due to the homogeneous nature of the i.i.d. setting).

AP	Before Personalized FL	After Personalized FL
1	68.676%	77.023%
2	68.676%	76.722%
3	68.676%	75.875%
4	68.676%	75.801%

TABLE IV: The global accuracy of each client device before and after fine-tuning, in the non-i.i.d. setting. We can see an increase in the global accuracy for each device after localized fine-tuning.

AP	Before Personalized FL	After Personalized FL
1	59.501%	88.386%
2	65.442%	97.571%
3	70.607%	87.827%
4	80.823%	94.310%

mitigate the low global performance typically seen in non i.i.d. RF fingerprinting environments.

Similar to Fig. 4, in Fig. 6, we show the global performance of FLAME in comparison to combinations of different modalities using $M = 2$ in the non i.i.d. setting. When compared with different combinations of modalities, FLAME still converges to a higher global accuracy. In addition, similar to trends seen in other signal environments, any modality combination containing Modality 2 performed very well, with the Modality 2 and Modality 3 combination performing very close to FLAME with $M = 3$. This reinforces our insights that Modality 2 possesses key features that allows for the training to perform much better than in the environments without it. It also reinforces our theoretical analysis by demonstrating the behavior of Theorem 1 and validating Assumption 2 and Assumption 3.

D. Personalized Federated Learning

We further aim to improve each AP's performance on the distribution of its data using personalized federated learning. Here, we train each local client on its local dataset, with the local models on each client device set to the weights of the global model obtained from at the conclusion of the federated training process. Then, we evaluate each local model's performance on a personalized testing set, which is a subset of the global testing data, consisting only of labels that are present in the training set.

Table III, in which we present the results of personalized training in an i.i.d setting, shows that the classification performance improves at each AP after personalized federated learning. Table IV, where we present the results of personalized FL in a non i.i.d. setting, shows that all APs improve in classification performance similar to the i.i.d. setting. Although the local models at all APs performed better after personalized FL, AP 2 two had the largest increase in performance, and the largest overall accuracy as well. Thus, we see that our proposed multimodal FL framework for RF fingerprinting can be further improved at each AP, in both i.i.d. and non i.i.d.

settings, via personalized FL to achieve the state-of-the-art classification performance of centralized deep learning.

V. CONCLUSION

In this paper, we proposed FLAME: a federated learning (FL) approach for multimodal RF fingerprinting. We showed that our proposed framework increases the convergence rate and overall global classification performance in a variety of federated learning settings when applied to fingerprinting data at multiple wireless access points (APs). We theoretically determined a convergence bound and empirically validated its efficacy on a real-world dataset. We then performed personalized federated learning and fine tuned the local model at each AP after the conclusion of the FL training rounds to maximize the fingerprinting classification performance on the distribution of data at each AP. In this setting, we showed that each AP benefits from a higher local accuracy after personalized federated learning is applied, thus making it a vital component of the FLAME framework. In future work, we anticipate extending our framework to consider its effectiveness on smaller and larger sets of transmitters. We also anticipate exploring the behavior of our derived convergence bound on out-of-distribution waveforms such as varying channel conditions and adversarial examples.

REFERENCES

- [1] V. Brik, S. Banerjee, M. Gruteser, and S. Oh, "Wireless device identification with radiometric signatures," in *Proceedings of the 14th ACM International Conference on Mobile Computing and Networking*, New York, NY, USA, 2008, p. 116–127.
- [2] S. Wang, R. Sahay, and C. G. Brinton, "How potent are evasion attacks for poisoning federated learning-based signal classifiers?" in *IEEE International Conference on Communications*, 2023, pp. 2376–2381.
- [3] T. Jian, B. C. Rendon, E. Ojuba, N. Soltani, Z. Wang, K. Sankhe, A. Gritsenko, J. Dy, K. Chowdhury, and S. Ioannidis, "Deep learning for rf fingerprinting: A massive experimental study," *IEEE Internet of Things Magazine*, vol. 3, no. 1, pp. 50–57, 2020.
- [4] K. Merchant, S. Revay, G. Stantchev, and B. Noursain, "Deep learning for rf device fingerprinting in cognitive communication networks," *IEEE Journal of Selected Topics in Signal Processing*, vol. 12, no. 1, pp. 160–167, 2018.
- [5] K. Sankhe, M. Belgiovine, F. Zhou, L. Angioloni, F. Restuccia, S. D'Oro, T. Melodia, S. Ioannidis, and K. Chowdhury, "No radio left behind: Radio fingerprinting through deep learning of physical-layer hardware impairments," *IEEE Transactions on Cognitive Communications and Networking*, vol. 6, no. 1, pp. 165–178, 2020.
- [6] Q. Wu, C. Feres, D. Kuzmenko, D. Zhi, Z. Yu, X. Liu, and X. 'Leo' Liu, "Deep learning based rf fingerprinting for device identification and wireless security," *Electronics Letters*, vol. 54, no. 24, pp. 1405–1407, 2018.
- [7] A. Otto, S. Rananga, and M. Masonta, "Deep learning vs. traditional learning for radio frequency fingerprinting," in *2024 IST-Africa Conference (IST-Africa)*, 2024, pp. 1–8.
- [8] R. W. Klein, M. A. Temple, and M. J. Mendenhall, "Application of wavelet-based rf fingerprinting to enhance wireless network security," *Journal of Communications and Networks*, vol. 11, no. 6, pp. 544–555, 2009.
- [9] J. Zhu, X. Luo, and D. Chen, "Maximum likelihood scheme for fingerprinting positioning in lte system," in *2012 IEEE 14th International Conference on Communication Technology*, 2012, pp. 428–432.
- [10] S. He, S.-H. G. Chan, L. Yu, and N. Liu, "Maxlifd: Joint maximum likelihood localization fusing fingerprints and mutual distances," *IEEE Transactions on Mobile Computing*, vol. 18, no. 3, pp. 602–617, 2019.
- [11] N. Nagia, M. T. Rahman, and S. Valaee, "Federated learning for wifi fingerprinting," in *IEEE International Conference on Communications*, 2022, pp. 4968–4973.

- [12] J. Shi, H. Zhang, S. Wang, B. Ge, S. Mao, and Y. Lin, "Fedrfid: Federated learning for radio frequency fingerprint identification of wifi signals," in *IEEE GLOBECOM*, 2022, pp. 154–159.
- [13] B. Gao, F. Yang, N. Cui, K. Xiong, Y. Lu, and Y. Wang, "A federated learning framework for fingerprinting-based indoor localization in multi-building and multifloor environments," *IEEE Internet of Things Journal*, vol. 10, no. 3, pp. 2615–2629, 2023.
- [14] Y. Zhao, M. Li, L. Lai, N. Suda, D. Civin, and V. Chandra, "Federated learning with non-iid data," *arXiv preprint arXiv:1806.00582*, 2018.
- [15] O. Shahid, S. Pouriyeh, R. M. Parizi, Q. Z. Sheng, G. Srivastava, and L. Zhao, "Communication efficiency in federated learning: Achievements and challenges," *arXiv preprint arXiv:2107.10996*, 2021.
- [16] O. Ureten and N. Serinken, "Wireless security through rf fingerprinting," *Canadian Journal of Electrical and Computer Engineering*, vol. 32, no. 1, pp. 27–33, 2007.
- [17] H. Yuan and A. Hu, "Preamble-based detection of wi-fi transmitter rf fingerprints," *Electronics Letters*, vol. 46, pp. 1165–1167, 2010.
- [18] L. Xiao, L. Greenstein, N. Mandayam, and W. Trappe, "A physical-layer technique to enhance authentication for mobile terminals," in *2008 IEEE International Conference on Communications*, 2008, pp. 1520–1524.
- [19] C. Bertoincini, K. Rudd, B. Noursain, and M. Hinders, "Wavelet fingerprinting of radio-frequency identification (rfid) tags," *IEEE Transactions on Industrial Electronics*, vol. 59, no. 12, pp. 4843–4850, 2012.
- [20] Z. Ren, P. Ren, and T. Zhang, "Deep rf device fingerprinting by semi-supervised learning with meta pseudo time-frequency labels," in *2022 IEEE Wireless Communications and Networking Conference (WCNC)*, 2022, pp. 2369–2374.
- [21] S. Halder and T. Newe, "Radio fingerprinting for anomaly detection using federated learning in lora-enabled industrial internet of things," *Future Generation Computer Systems*, vol. 143, pp. 322–336, 2023.
- [22] P. Qi, X. Zhou, S. Zheng, and Z. Li, "Automatic modulation classification based on deep residual networks with multimodal information," *IEEE Transactions on Cognitive Communications and Networking*, vol. 7, no. 1, pp. 21–33, 2021.
- [23] K. Triaridis, C. Doumanidis, N. D. Chatzidiamantis, and G. K. Karagiannidis, "Mm-net: A multi-modal approach toward automatic modulation classification," *IEEE Communications Letters*, vol. 28, no. 2, pp. 328–331, 2024.
- [24] R. Sahay, C. G. Brinton, and D. J. Love, "A deep ensemble-based wireless receiver architecture for mitigating adversarial attacks in automatic modulation classification," *IEEE Transactions on Cognitive Communications and Networking*, vol. 8, no. 1, pp. 71–85, 2022.
- [25] K. Yang, J. Kang, J. Jang, and H.-N. Lee, "Multimodal sparse representation-based classification scheme for rf fingerprinting," *IEEE Communications Letters*, vol. 23, no. 5, pp. 867–870, 2019.
- [26] W. Huang, D. Wang, X. Ouyang, J. Wan, J. Liu, and T. Li, "Multimodal federated learning: Concept, methods, applications and future directions," *Information Fusion*, vol. 112, p. 102576, 2024.
- [27] Y. Zhao, P. Barnaghi, and H. Haddadi, "Multimodal federated learning on iot data," in *2022 IEEE/ACM Seventh International Conference on Internet-of-Things Design and Implementation (IoTDI)*, 2022, pp. 43–54.
- [28] P. Qi, D. Chiaro, and F. Piccialli, "Fl-fid: Federated learning-based fall detection with multimodal data fusion," *Information Fusion*, vol. 99, p. 101890, 2023.
- [29] M. Kulin, T. Kazaz, I. Moerman, and E. De Poorter, "End-to-end learning from spectrum data: A deep learning approach for wireless signal identification in spectrum monitoring applications," *IEEE Access*, vol. 6, pp. 18484–18501, 2018.
- [30] T. J. O'Shea, T. Roy, and T. C. Clancy, "Over-the-air deep learning based radio signal classification," *IEEE Journal of Selected Topics in Signal Processing*, vol. 12, no. 1, pp. 168–179, 2018.
- [31] S. Hanna, S. Karunaratne, and D. Cabric, "Open set wireless transmitter authorization: Deep learning approaches and dataset considerations," *IEEE Transactions on Cognitive Communications and Networking*, vol. 7, no. 1, pp. 59–72, 2021.
- [32] S. S. Hanna and D. Cabric, "Deep learning based transmitter identification using power amplifier nonlinearity," in *International Conference on Computing, Networking and Communications (ICNC)*, 2019, pp. 674–680.
- [33] C. Morin, L. S. Cardoso, J. Hoydis, J.-M. Gorce, and T. Vial, "Transmitter classification with supervised deep learning," in *14th EAI International Conference, CrownCom 2019, Poznan, Poland, June 11–12, 2019, Proceedings 14*. Springer, 2019, pp. 73–86.
- [34] K. He, X. Zhang, S. Ren, and J. Sun, "Deep residual learning for image recognition," in *Proceedings of the IEEE conference on computer vision and pattern recognition*, 2016, pp. 770–778.

APPENDIX

A. Proof of Lemma 1

Proof. We aim to represent $\nabla f_n(\mathbf{w}_n^{(t,j)})$, which denotes the local model at AP n after j local SGD steps, in terms of the global loss gradient $\nabla f(\mathbf{w}^{(t)})$ as well as terms capturing deviations of the loss. In this regard, the local loss contains three sources of deviations: (1) the gradient of the global loss, $\nabla f(\mathbf{w}^{(t)})$, which captures the direction minimizing the global objective $f(\mathbf{w})$; (2) the local drift $\nabla f_n(\mathbf{w}_n^{(t,j)}) - \nabla f_n(\mathbf{w}^{(t)})$, which captures the deviation of the loss gradient induced from performing SGD over random mini-batches at each AP before global aggregation; and (3) gradient heterogeneity $\nabla f_n(\mathbf{w}_n^{(t,j)}) - \nabla f(\mathbf{w}^{(t)})$, which is induced by the unique data distribution at each AP. Accounting for the deviation to the local loss gradient from these sources, we can decompose the local loss as shown in (9) to capture the impact of each source on overall convergence. \square

B. Proof of Theorem 1

Proof. Using the L -Lipschitz smoothness of $f(\mathbf{w})$, we have

$$f(\mathbf{w}^{(t+1)}) \leq f(\mathbf{w}^{(t)}) + \langle \nabla f(\mathbf{w}^{(t)}), \mathbf{w}^{(t+1)} - \mathbf{w}^{(t)} \rangle + \frac{L}{2} \|\mathbf{w}^{(t+1)} - \mathbf{w}^{(t)}\|^2. \quad (11)$$

Given that local parameter updates are given by (7), the final local model after J SGD steps is given by

$$\mathbf{w}_n^{(t,J)} = \mathbf{w}^{(t)} - \eta \sum_{j=0}^{J-1} \nabla f_n(\mathbf{w}_n^{(t,j)}). \quad (12)$$

Substituting (12) into the parameter update expression in (8), we see that

$$\begin{aligned} \mathbf{w}^{(t+1)} &= \frac{1}{N} \sum_{n=1}^N \left(\mathbf{w}^{(t)} - \eta \sum_{j=0}^{J-1} \nabla f_n(\mathbf{w}_n^{(t,j)}) \right) \\ &= \mathbf{w}^{(t)} - \frac{\eta}{N} \sum_{n=1}^N \sum_{j=0}^{J-1} \nabla f_n(\mathbf{w}_n^{(t,j)}), \end{aligned} \quad (13)$$

and thus

$$\mathbf{w}^{(t+1)} - \mathbf{w}^{(t)} = -\frac{\eta}{N} \sum_{n=1}^N \sum_{j=0}^{J-1} \nabla f_n(\mathbf{w}_n^{(t,j)}). \quad (14)$$

Substituting (14) into the smoothness inequality from (11), we arrive at

$$\begin{aligned} f(\mathbf{w}^{(t+1)}) &\leq \\ &f(\mathbf{w}^{(t)}) - \eta \left\langle \nabla f(\mathbf{w}^{(t)}), \frac{1}{N} \sum_{n=1}^N \sum_{j=0}^{J-1} \nabla f_n(\mathbf{w}_n^{(t,j)}) \right\rangle \\ &\quad + \frac{L}{2} \left\| -\frac{\eta}{N} \sum_{n=1}^N \sum_{j=0}^{J-1} \nabla f_n(\mathbf{w}_n^{(t,j)}) \right\|^2. \end{aligned} \quad (15)$$

The inner product can be written as

$$-\eta \left\langle \nabla f(\mathbf{w}^{(t)}), \frac{1}{N} \sum_{n=1}^N \sum_{j=0}^{J-1} \nabla f_n(\mathbf{w}_n^{(t,j)}) \right\rangle$$

$$= -\frac{\eta}{N} \sum_{n=1}^N \sum_{j=0}^{J-1} \langle \nabla f(\mathbf{w}^{(t)}), \nabla f_n(\mathbf{w}_n^{(t,j)}) \rangle, \quad (16)$$

which we substitute into Lemma 1 and arrive at

$$\begin{aligned} \langle \nabla f(\mathbf{w}^{(t)}), \nabla f_n(\mathbf{w}_n^{(t,j)}) \rangle &= \|\nabla f(\mathbf{w}^{(t)})\|^2 \\ &+ \langle \nabla f(\mathbf{w}^{(t)}), \nabla f_n(\mathbf{w}_n^{(t,j)}) - \nabla f_n(\mathbf{w}_n) \rangle \\ &+ \langle \nabla f(\mathbf{w}^{(t)}), \nabla f_n(\mathbf{w}^{(t)}) - \nabla f(\mathbf{w}^{(t)}) \rangle. \end{aligned} \quad (17)$$

Bounding each term in (17), we have

$$\sum_{n=1}^N \sum_{j=0}^{J-1} \|\nabla f(\mathbf{w}^{(t)})\|^2 = NJ \|\nabla f(\mathbf{w}^{(t)})\|^2 \quad (18)$$

for the first term. From the Cauchy-Schwarz inequality, we have

$$\begin{aligned} &\langle \nabla f(\mathbf{w}^{(t)}), \nabla f_n(\mathbf{w}_n^{(t,j)}) - \nabla f_n(\mathbf{w}_n) \rangle \\ &\leq \|\nabla f(\mathbf{w}^{(t)})\| \cdot \|\nabla f_n(\mathbf{w}_n^{(t,j)}) - \nabla f_n(\mathbf{w}_n)\|, \end{aligned} \quad (19)$$

and, from Assumption 2, we can bound (19) according to

$$\mathbb{E}[\|\nabla f_n(\mathbf{w}_n^{(t,j)}) - \nabla f_n(\mathbf{w}_n)\|^2] \leq \frac{\sigma^2}{M} \quad (20)$$

for the second term. Similarly, for the third term, we have

$$\begin{aligned} &\langle \nabla f(\mathbf{w}^{(t)}), \nabla f_n(\mathbf{w}^{(t)}) - \nabla f(\mathbf{w}^{(t)}) \rangle \\ &\leq \|\nabla f(\mathbf{w}^{(t)})\| \cdot \|\nabla f_n(\mathbf{w}^{(t)}) - \nabla f(\mathbf{w}^{(t)})\|, \end{aligned} \quad (21)$$

and, from Assumption 3, we can bound (21) according to

$$\mathbb{E}[\|\nabla f_n(\mathbf{w}^{(t)}) - \nabla f(\mathbf{w}^{(t)})\|^2] \leq \frac{\zeta^2}{M}. \quad (22)$$

Next, we expand the norm term from (15) and see that

$$\begin{aligned} \|\mathbf{w}^{(t+1)} - \mathbf{w}^{(t)}\|^2 &= \left\| -\frac{\eta}{N} \sum_{n=1}^N \sum_{j=0}^{J-1} \nabla f_n(\mathbf{w}_n^{(t,j)}) \right\|^2 \\ &= \frac{\eta^2}{N^2} \left\| \sum_{n=1}^N \sum_{j=0}^{J-1} \nabla f_n(\mathbf{w}_n^{(t,j)}) \right\|^2 \\ &= \frac{\eta^2}{N^2} (NJ \|\nabla f(\mathbf{w}^{(t)})\|^2 + \text{variance terms}), \end{aligned} \quad (23)$$

where the variance terms are bounded σ^2/M and ζ^2/M as shown in (20) and (22), respectively. Finally, substituting the bounds of (17) as well as (23) into the smoothness inequality from (15), we arrive at

$$f(\mathbf{w}^{(t+1)}) \leq f(\mathbf{w}^{(t)}) - \eta J \|\nabla f(\mathbf{w}^{(t)})\|^2 + \frac{\eta^2 L J^2 (\sigma^2 + \zeta^2)}{2NM}, \quad (24)$$

which can be rewritten in terms of the optimal loss f^* :

$$\begin{aligned} \mathbb{E}[f(\mathbf{w}^{(t+1)}) - f^*] &\leq \mathbb{E}[f(\mathbf{w}^{(t)}) - f^*] \left(1 - \frac{\eta J \mu}{M} \right) \\ &\quad + \frac{\eta^2 L J^2 (\sigma^2 + \zeta^2)}{2NM}. \end{aligned} \quad (25)$$

□